Applied Ocean Research 139 (2023) 103711

Contents lists available at ScienceDirect

Applied Ocean Research

journal homepage: www.elsevier.com/locate/apor

Research paper

Stochastic analysis of the nonlinear dynamics of oscillating water columns: A frequency domain approach

L.S.P. da Silva [a,b,e,*], C.P. Pesce [c], M. de Oliveira [d], N.Y. Sergiienko [b], B. Cazzolato [b], B. Ding [b]

[a] Delmar Systems, Perth, Australia
[b] The University of Adelaide, School of Mechanical Engineering, Australia
[c] University of São Paulo, Escola Politécnica, Dept. of Ocean Engineering and Offshore Mechanics Laboratory, Brazil
[d] University of São Paulo, Escola Politécnica, Dept. of Mechanical Engineering, Brazil
[e] University of São Paulo, Institute of Mathematics and Computer Sciences, Brazil

ARTICLE INFO

Keywords:
Oscillating Water Column
Moon pools
Statistical Quadratisation
Stochastic Analysis
Nonlinear Dynamics

ABSTRACT

This paper investigates the first and second-order stochastic responses of oscillating water columns (OWCs) under random waves. The OWCs' nonlinear dynamics are computed in the frequency domain, where sources of nonlinearities are replaced by equivalent polynomial terms up to second order by minimising their difference in a mean-square sense. This procedure is known as the statistical quadratisation (SQ) technique. In such an approach, the linear and quadratic coefficients are obtained using an iterative procedure and non-Gaussian distributions based on Gram–Charlier expansions, and the dynamics are solved using the Volterra theory. The results are compared against a statistical linearisation model (SL), and nonlinear time-domain simulations (TD) to illustrate the capabilities of the method. The result demonstrated an excellent agreement for the first and second-order motions of the water column obtained using statistical quadratisation compared to nonlinear time-domain simulations in terms of spectral response and probability distribution. Along with the good accuracy, the statistical quadratisation has the advantage of being approximately two orders of magnitude faster than nonlinear time-domain simulations. For the proposed systems, the nonlinearity from the variable mass system (inertial type) is shown to be the most important source of second-order effects driving the oscillating water column dynamics based on the environmental conditions and drafts investigated in this work.

1. Introduction

Oscillating water columns (OWCs) have been extensively applied in the offshore engineering field. For Oil & Gas (O&G) platforms and vessel applications, OWCs are usually referred to as moon pools and are designed to give special protection during the installation and maintenance of subsea equipment, and improve the response of the floating structure (Masetti et al., 2012; Guo et al., 2017). More recently, the same principle has been extended to the renewable energy field in the platform concepts of floating offshore wind turbines (FOWTs) (Chuang et al., 2021). For instance, the Floatgen concept used by BW Ideol consists of a barge platform with a Damping pool® system to improve the platform's response (Ideol, 2022). Moon pools have also been investigated in barge FOWTs to accommodate aquaculture fish cages (Li et al., 2020). Different use of OWCs occurs when designing wave energy converters (WECs), where the OWC is set to operate in resonance to increase the energy transfer from waves to the power take-off mechanism, which are composed of air turbines (Falcão and Henriques, 2016). Hence, the natural frequency of the OWC is set to be close to the dominant wave peak frequency of the site for wave energy applications (Silva et al., 2020). As observed, the OWC dynamics vary with its use (motion suppression or energy extraction), and reliable estimations of the response are required regardless of the purpose (Sanchez-Mondragon et al., 2017).

The OWCs dynamics is a fundamental problem in the field of hydrodynamics, and it can be described as a variable mass system based on the piston-like mode (Pesce et al., 2023; Aalbers, 1984; Spanos et al., 2018). The OWC is subjected to random excitations from irregular sea states, and its dynamics are commonly simulated using time-domain models due to the existence of nonlinear forces. However, during preliminary design stages, several environmental conditions and OWC configurations are usually investigated. Hence, efficient methods of estimating the nonlinear response of the water column under random excitations are beneficial (Davidson and Costello, 2020). In this regard, statistical linearisation (SL) is one of the most useful, versatile, and fast methods to estimate nonlinear system responses under

* Corresponding author at: The University of Adelaide, School of Mechanical Engineering, Australia.
E-mail address: leandropinheiro@alumni.usp.br (L.S.P. da Silva).

https://doi.org/10.1016/j.apor.2023.103711
Received 24 April 2023; Received in revised form 30 July 2023; Accepted 21 August 2023
Available online 6 September 2023

random excitations (Spanos, 1981). The SL method is built upon the frequency-domain model and approximates the nonlinear response to an equivalent linear one, where the difference between both equations is minimised in a mean squared sense. The SL has been applied to a variety of offshore systems, such as oil and gas platforms (Spanos et al., 2005), floating offshore wind turbines (da Silva et al., 2022b; Karimi et al., 2019; da Silva et al., 2022c), while examples of SL applied to OWCs can be found in Spanos et al. (2018, 2011), da Silva (2019), Silva et al. (2019), Scialò et al. (2022) and Folley and Whittaker (2013), and arrays of OWCs in Malara and Spanos (2019). For a survey of the method, the reader is encouraged to read the material presented in da Silva (2023), Roberts and Spanos (2003) and Socha (2008, 2005a,b).

The SL approach usually offers a reasonable estimate of the mean and mean square response; however, there are limitations. The SL is restricted to the response within the primary excitation spectrum range, and the probability distribution is generally limited to Gaussian distributions (Folley, 2016). It is well-known that nonlinearities can cause vibrations outside the primary excitation frequency range, and in practice, the response may be better represented by a non-Gaussian distribution. Hence, SL models might lose the representativeness of the actual nonlinear dynamics. These limitations can be circumvented by replacing the nonlinear function with an equivalent quadratic one by means of the statistical quadratisation (SQ) method (Donley and Spanos, 1990; Spanos and Donley, 1991; Silva et al., 2021), which can be considered as an extension of the SL with high-order Volterra series. In this regard, the Non-Gaussian distribution can be estimated from the central moments via direct integration in the frequency domain and using Gram–Charlier expansions of the Gaussian distribution (Bedrosian and Rice, 1971). The works in Donley and Spanos (1990), Spanos and Donley (1991) and Silva et al. (2021) applied SQ to flow-related vibration of structures, which is conceptually similar to the OWC problem. As a result, the application of SQ can be an effective tool to estimate and understand the nonlinear behaviour of OWCs.

The following work assesses the resonant behaviour of the water column dynamics inside the pipe under the action of random waves by means of the SQ technique. The paper is structured as follows. Firstly, the SQ model of the OWC under first and second-order loads is introduced based on derivations presented in Pesce et al. (2023). Then, an SL model considering only linear excitation forces is briefly introduced for comparison purposes (Silva et al., 2020). The frequency-domain-based models are compared against the full nonlinear time-domain (TD) model to verify the reliability of each method. Several OWCs designs and environmental conditions are investigated to demonstrate the sensitivity of the responses. Finally, a discussion is made regarding the main sources of non-linearities (first and second-order effects), simulation time, capability, and limitation of each method. The conclusion section summarises the main outcomes of the paper.

To the best of the authors' knowledge, the use of SQ has not been applied yet to analyse the OWC dynamics, which has a huge potential to circumvent the limitations of SL results (da Silva et al., 2022a; Folley, 2016). Note that the statistical quadratisation can be further extended to include third-order responses by using statistical cubicisation (SC) (Tognarelli et al., 1997a,b). The application of SQ and SC methods to offshore systems remains insufficiently explored, and some examples can be found in Silva et al. (2021), Li et al. (1995) and Quek et al. (1994).

2. Random vibration of oscillating water columns

The nonlinear dynamics of an OWC can be derived based on the plug flow hypothesis of an incompressible fluid, where the free surface inside the pipe (ζ) is considered as the only generalised coordinate of the system, and it is measured from the undisturbed free surface outside the pipe, as demonstrated in Pesce et al. (2023). The OWC is assumed to be fixed and its dynamics are characterised by a variable mass system with an explicit dependency on the position of the inner free surface.

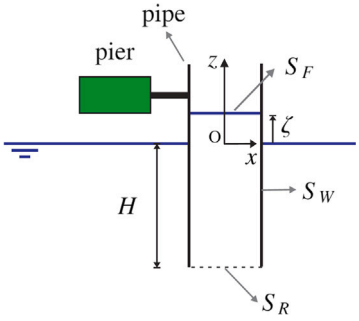

Fig. 1. Sketch of the water column system based on (Pesce et al., 2023).

Fig. 1 illustrates the fixed water column problem investigated in this paper, which is composed of a cylindrical-shaped structure piercing the seawater. Note that, in this case of a pipe with a constant cross-section, the mass inside the pipe is linearly dependent on the generalised coordinate ζ. The region of interest encloses the non-material volume defined by the surface $S : S_F \cup S_W \cup S_R$, where S_F and S_W denote the free-surface and wall surface (material surfaces); and S_R denotes the inlet/outlet surface (non-material control surface), across which there are fluxes of mass, momentum and kinetic energy. Pressure is assumed null at S_F, as the pipe is here supposed open to the atmosphere. However, in WEC applications, the air chamber thermodynamics and the power take-off system must be included in the dynamics. The full derivation of the reduced order model for the water column dynamics is beyond the scope of this paper, and the reader is encouraged to consult Ref. Pesce et al. (2023), where the governing equation is obtained via two main and equivalent approaches: the extended Lagrange Equations applied to mechanical systems with mass dependent on position (Pesce, 2003), and/or applying the Extended Hamilton's Principle for non-material volumes (Casetta and Pesce, 2013). A full discussion can be found in Pesce et al. (2023) on subtle theoretical points concerning the applications of those two fundamental results to the present problem.

2.1. Statistical quadratisation

Following the results presented in Pesce et al. (2023), the water column dynamics forced by a train of incident linear free surface waves can be described as[1]:

$$(\zeta + H)\ddot{\zeta} + C(\zeta + H)\dot{\zeta} + \frac{1}{2}C_V\dot{\zeta}\,|\dot{\zeta}| + g\zeta = g\xi - \left[\varphi_{w_t} + \frac{1}{2}\varphi_{w_x}^2\right]_{S_R}, \tag{1}$$

with,

$$\varphi_w(x,z,t) = \sum_{j=1}^{N_\omega} \frac{\omega_j a_j}{k_j} \frac{\cosh(k_j(z+h))}{\sinh k_j h} \sin(k_j x - \omega_j t), \tag{2}$$

$$\xi(x,t) = \sum_{j=1}^{N_\omega} a_j \cos(k_j x - \omega_j t), \tag{3}$$

$$\omega_j^2 = g k_j \tanh k_j h, \tag{4}$$

where ξ denotes the wave surface elevation, a_j is the amplitude of jth frequency component of the wave surface elevation, N_w the total number of wave frequencies used to compute the wave spectrum, k is the wave number, g is the gravitational acceleration, H is the nominal water column draft; the incident wave velocity potential, φ_w, and its derivatives with respect to time and the coordinate x are given respectively by φ_{w_t} and φ_{w_x}, which are computed at the centre of the non-material control surface S_R; C denotes a linear damping

[1] A discussion on the field velocity at SR may be found in Pesce et al. (2023).

coefficient. This ansatz takes a simple Rayleighian-like model, in which damping is supposed to be linearly proportional to the varying mass inside the pipe. The quadratic damping term is added to emulate the viscous losses effects at the mouth of the pipe, where C_V is an ad-hoc and heuristic damping coefficient that here is assumed to be given by a two-valued coefficient, in order to describe the asymmetry between the viscous losses of the out-going and in-going fluid at S_R. An assessment of such a simple model regarding the viscous losses effects at the mount (S_R) and the Rayleighian-like model might be done through computational fluid dynamic simulations and experimental tests. However, in the spirit of the present paper, this task is left to further work, so the coefficients C and C_V are here treated as known parameters.

Notice that the free surface piercing pipe is here considered fixed. Moreover, diffracted waves are not taken into account for the sake of simplicity. Physically this means that the diameter of the pipe is considered small compared to the incident wavelength. Linear diffraction effects, e.g. Li and Liu (2019), could be considered in a more complete analytical model; even second-order diffraction effects could be conceived in a semi-analytical way, Taylor and Huang (1997). However, this would impair a prompt understanding of the present paper, whose main objective is to assess the capability of the SQ model to tackle the nonlinear dynamics of the OWC, which dynamic is considered modelled by a simple potential plug flow type, as discussed in Pesce et al. (2023).

In the OWC dynamics, the mean surface elevation differs from the unperturbed condition due to the non-symmetric nonlinearities, such as the ones from the quadratic terms. Thus, the stationary response of the water column displacement can be expressed as:

$$\zeta(t) = \mu_\zeta + \hat{\zeta}(t), \tag{5}$$

where μ_ζ denotes the mean water column surface displacement, and $\hat{\zeta}$ denotes the (supposedly) stationary, non-Gaussian, and zero mean process of the water column surface displacement. Rearranging Eq. (1) and expressing the dynamics as in Eq. (5), the governing equation of the water column dynamics can be expressed as:

$$H\ddot{\hat{\zeta}}+CH\dot{\hat{\zeta}}+g\left(\mu_\zeta+\hat{\zeta}\right)=g\hat{\xi}-\left[\varphi_{w_t}+\frac{1}{2}\varphi_{w_x}^2\right]_{S_R}-\zeta\ddot{\hat{\zeta}}-C\zeta\dot{\hat{\zeta}}-\frac{1}{2}C_V\dot{\hat{\zeta}}\left|\dot{\hat{\zeta}}\right|, \tag{6}$$

where the left-hand side is given by a linear operator, and the mean surface displacement can be estimated by taking the expectation of Eq. (6) as:

$$\mu_\zeta = g^{-1}\left\langle\left[-\frac{1}{2}\varphi_{w_x}^2\right]_{S_R}-\zeta\ddot{\hat{\zeta}}-\frac{1}{2}C_V\dot{\hat{\zeta}}\left|\dot{\hat{\zeta}}\right|\right\rangle, \tag{7}$$

where $\langle\ \rangle$ denotes the mathematical expectation. Note that the quadratic nonlinearity given by $C\zeta\dot{\hat{\zeta}}$ is not included in the expectation of the mean water column surface displacement because for stationary responses $\left\langle\zeta\dot{\hat{\zeta}}\right\rangle = 0$, and the quadratic damping at the water column mouth produces a mean force due to the assumption of a two-valued C_V coefficient.

Hereafter, it is important to notice that most nonlinearities present in the OWCs dynamics are written in the polynomial form up to the second order, with the exception of the quadratic damping term. The polynomial representation allows writing the dynamics by means of the Volterra series. In this regard, the nonlinear damping is approximated by equivalent linear and quadratic terms with respect to the velocity based on the statistical quadratisation procedure (Donley and Spanos, 1990):

$$\frac{1}{2}C_V\dot{\hat{\zeta}}\left|\dot{\hat{\zeta}}\right| \approx C_{eq,lin}\dot{\hat{\zeta}} + C_{eq,quad}\left(\dot{\hat{\zeta}}^2 - \left\langle\dot{\hat{\zeta}}^2\right\rangle\right). \tag{8}$$

Note that the quadratic term is null for the case of a single-valued C_V coefficient, which produces a symmetric nonlinearity, and the equivalent linear system can be obtained by means of statistical linearisation. The method of statistical quadratisation consists in minimising the difference between the nonlinear load and its equivalent linear and quadratic one in a mean square sense:

$$\min\left\langle\varepsilon^2\right\rangle, \tag{9}$$

where ε is defined as the difference between the right and left-hand side of Eq. (8):

$$\varepsilon = \frac{1}{2}C_V\dot{\hat{\zeta}}\left|\dot{\hat{\zeta}}\right| - C_{eq,lin}\dot{\hat{\zeta}} - C_{eq,quad}\left(\dot{\hat{\zeta}}^2 - \left\langle\dot{\hat{\zeta}}^2\right\rangle\right). \tag{10}$$

Defining $\underline{\dot{\zeta}}^{\mathrm{T}} = \left(\dot{\hat{\zeta}}, \dot{\hat{\zeta}}^2 - \left\langle\dot{\hat{\zeta}}^2\right\rangle\right)$, it can be demonstrated that the required condition to minimise the difference, given in Eq. (10), can be achieved by the following operation:

$$\left\langle\underline{\dot{\zeta}}\,\underline{\dot{\zeta}}^{\mathrm{T}}\right\rangle\underline{C}_{eq} = \left\langle\frac{1}{2}C_V\dot{\hat{\zeta}}\left|\dot{\hat{\zeta}}\right|\underline{\dot{\zeta}}\right\rangle, \tag{11}$$

where:

$$\begin{aligned}\left\langle\underline{\dot{\zeta}}\,\underline{\dot{\zeta}}^{\mathrm{T}}\right\rangle &= \begin{bmatrix}\mu_{\dot{\zeta}^2} & \mu_{\dot{\zeta}^3}\\ \mu_{\dot{\zeta}^3} & \mu_{\dot{\zeta}^4}-\left(\mu_{\dot{\zeta}^2}\right)^2\end{bmatrix},\\ \underline{C}_{eq} &= \begin{Bmatrix}C_{\mathrm{eq,lin}}\\ C_{\mathrm{eq,quad}}\end{Bmatrix},\\ \left\langle\frac{1}{2}C_V\dot{\hat{\zeta}}\left|\dot{\hat{\zeta}}\right|\underline{\dot{\zeta}}\right\rangle &= \begin{Bmatrix}\left\langle\frac{1}{2}C_V\dot{\hat{\zeta}}\left|\dot{\hat{\zeta}}\right|\dot{\hat{\zeta}}\right\rangle\\ \left\langle\frac{1}{2}C_V\dot{\hat{\zeta}}\left|\dot{\hat{\zeta}}\right|\dot{\hat{\zeta}}^2\right\rangle - \left\langle\frac{1}{2}C_V\dot{\hat{\zeta}}\left|\dot{\hat{\zeta}}\right|\right\rangle\mu_{\dot{\zeta}^2}\end{Bmatrix}.\end{aligned} \tag{12}$$

The expectation in the left-hand side of Eq. (11) involves joint central moments of the water column surface velocity, while the right-hand side terms are calculated using a non-Gaussian distribution, which can be estimated based on the procedures described in Sections 2.1.1 and 2.1.2.

Subtracting the mean surface displacement from Eq. (6) and using the equivalent quadratic term described in Eq. (8), the zero-mean random water column surface displacement can be obtained as:

$$\begin{aligned}H\ddot{\hat{\zeta}} + \left(CH + C_{eq,lin}\right)\dot{\hat{\zeta}} + g\hat{\zeta} = g\hat{\xi} &- \left[\varphi_{w_t} + \frac{1}{2}\varphi_{w_x}^2\right]_{S_R} - \hat{\zeta}\ddot{\hat{\zeta}}\\ &- C\hat{\zeta}\dot{\hat{\zeta}} - C_{eq,quad}\dot{\hat{\zeta}}^2,\\ &+ \left\langle\left[\frac{1}{2}\varphi_{w_x}^2\right]_{S_R} + \hat{\zeta}\ddot{\hat{\zeta}} + C_{eq,quad}\left\langle\dot{\hat{\zeta}}^2\right\rangle\right\rangle.\end{aligned} \tag{13}$$

Hereafter, the system dynamics is expressed in a polynomial form, which is suitable for the Volterra series method. Based on that, the solution of water column surface displacement is assumed to be represented by an infinite Volterra series as:

$$\hat{\zeta}(t) = \sum_{p=1}^{\infty}\lambda^p\hat{\zeta}^{(p)}(t), \tag{14}$$

where terms up to $p = 2$ are accounted for in this work to characterise the quadratic effects, and λ is a scalar coefficient equal to one that is introduced for bookkeeping purposes. Assuming that the excitation forces can also be expressed using the Volterra series and equating terms with the same power of λ, the water column surface displacement dynamics can be represented by two linear systems as:

$$H\ddot{\hat{\zeta}}^{(1)} + \left(CH + C_{eq,lin}\right)\dot{\hat{\zeta}}^{(1)} + g\hat{\zeta}^{(1)} = g\xi^{(1)} - \left[\varphi_{w_t}^{(1)}\right]_{S_R}, \tag{15}$$

$$\begin{aligned}&H\ddot{\hat{\zeta}}^{(2)} + \left(CH + C_{eq,lin}\right)\dot{\hat{\zeta}}^{(2)} + g\hat{\zeta}^{(2)}\\ &= -\left[\frac{1}{2}\varphi_{w_x}^{(1)2}\right]_{S_R} - \hat{\zeta}^{(1)}\ddot{\hat{\zeta}}^{(1)} - C\hat{\zeta}^{(1)}\dot{\hat{\zeta}}^{(1)} - C_{eq,quad}\dot{\hat{\zeta}}^{(1)2}\\ &+ \left\langle\left[\frac{1}{2}\varphi_{w_x}^{(1)2}\right]_{S_R} + \hat{\zeta}^{(1)}\ddot{\hat{\zeta}}^{(1)} + C_{eq,quad}\dot{\hat{\zeta}}^{(1)2}\right\rangle,\end{aligned} \tag{16}$$

Note that Eqs. (15) and (16) are intertwined because the second-order response depends on the first-order response, while the equivalent linear and quadratic damping coefficients depend on the entire response. Nevertheless, both equations have the same linear differential operator. Hence, these two equations can be combined into a single system, and the water column surface displacement can be expressed as:

$$H\ddot{\hat{\zeta}} + \left(CH + C_{eq,lin}\right)\dot{\hat{\zeta}} + g\hat{\zeta} = \hat{\mathrm{f}} = \hat{\mathrm{f}}^{(0)} + \hat{\mathrm{f}}^{(1)} + \hat{\mathrm{f}}^{(2)}, \tag{17}$$

where the linear operator on the right-hand side is excited up to the second order. The forcing terms in Eq. (17) can be described as a Volterra series in the form:

$$\begin{aligned} \mathrm{f}(t) = \hat{\mathrm{f}}^{(0)} &+ \int_{-\infty}^{\infty} \mathrm{h}_f^{(1)}(\tau_1)\xi(t-\tau_1)d\tau_1 \\ &+ \int_{-\infty}^{\infty}\int_{-\infty}^{\infty} \mathrm{h}_f^{(2)}(\tau_1,\tau_2)\xi(t-\tau_1)\xi(t-\tau_2)d\tau_1 d\tau_2, \end{aligned} \tag{18}$$

where $\mathrm{h}_f^{(1)}(\tau_1)$ and $\mathrm{h}_f^{(2)}(\tau_1,\tau_2)$ denote the linear and quadratic Volterra kernels for the forcing function, also referred to as linear and quadratic impulse response functions of the forcing terms. The linear and quadratic kernels of forcing terms acting on the OWC can be expressed in terms of transfer functions by the following Fourier transform:

$$\mathrm{H}_{\hat{\mathrm{f}}}^{(1)}(\omega) = g\left(1+\omega^2\frac{\cosh k(h-H)}{\cosh kh}\right), \tag{19}$$

and,

$$\begin{aligned} \mathrm{H}_{\hat{\mathrm{f}}}^{(2)}(\omega_1,\omega_2) = &-\frac{1}{2}\mathrm{H}_{\varphi_{w,x}}^{(1)}(\omega_1)\mathrm{H}_{\varphi_{w,x}}^{(1)}(\omega_2) + C_{eq,quad}\omega_1\omega_2\mathrm{H}_{\hat{\zeta}}^{(1)}(\omega_1)\mathrm{H}_{\hat{\zeta}}^{(1)}(\omega_2) \\ &- \frac{C}{2}i(\omega_1+\omega_2)\mathrm{H}_{\hat{\zeta}}^{(1)}(\omega_1)\mathrm{H}_{\hat{\zeta}}^{(1)}(\omega_2) \\ &+ \frac{1}{2}\left(\omega_1^2+\omega_2^2\right)\mathrm{H}_{\hat{\zeta}}^{(1)}(\omega_1)\mathrm{H}_{\hat{\zeta}}^{(1)}(\omega_2), \end{aligned} \tag{20}$$

with:

$$\mathrm{H}_{\varphi_{w,x}}^{(1)}(\omega) = \omega\frac{\cosh k(h+H)}{\sinh kh}, \tag{21}$$

where h is the water depth, and k denotes the wavenumber, which is obtained by solving the transcendental equation given by the linear dispersion relation:

$$\omega^2 = gk\tanh kh. \tag{22}$$

Note that the quadratic kernel in Eq. (20) was written in a symmetric form to reduce the computational effort and storage requirements in further calculations, as recommended in Donley and Spanos (1990). Since the operator in Eq. (17) has a linear form, the response can be written in a similar form:

$$\begin{aligned} \hat{\zeta}(t) = \hat{\zeta}^{(0)} + \hat{\zeta}^{(1)} + \hat{\zeta}^{(2)} &= \hat{\zeta}^{(0)} + \int_{-\infty}^{\infty} \mathrm{h}_{\hat{\zeta}}^{(1)}(\tau_1)\xi(t-\tau_1)d\tau_1 \\ &+ \int_{-\infty}^{\infty}\int_{-\infty}^{\infty} \mathrm{h}_{\hat{\zeta}}^{(2)}(\tau_1,\tau_2)\xi(t-\tau_1)\xi(t-\tau_2)d\tau_1 d\tau_2, \end{aligned} \tag{23}$$

where the linear and quadratic Volterra kernels for the water column surface displacement, $\mathrm{h}_{\hat{\zeta}}^{(1)}(\tau_1)$ and $\mathrm{h}_{\hat{\zeta}}^{(2)}(\tau_1,\tau_2)$, are also described using transfer functions as:

$$\mathrm{H}_{\hat{\zeta}}^{(1)}(\omega) = \mathrm{H}(\omega)\mathrm{H}_{\hat{\mathrm{f}}}^{(1)}(\omega), \tag{24}$$

and,

$$\mathrm{H}_{\hat{\zeta}}^{(2)}(\omega_1,\omega_2) = \mathrm{H}(\omega_1+\omega_2)\mathrm{H}_{\hat{\mathrm{f}}}^{(2)}(\omega), \tag{25}$$

where:

$$\mathrm{H}(\omega) = \left[-\omega^2 H + i\omega\left(CH + C_{eq,lin}\right) + g\right]^{-1}. \tag{26}$$

2.1.1. Probability distribution

The probability response distribution offers relevant characteristics of the dynamics under random vibrations, and in this study, the probability distribution is also necessary to estimate the equivalent linear and quadratic system, as shown in Eq. (11). However, obtaining the probability distribution of nonlinear systems is a non-trivial task. Although the wave surface elevation can be assumed to be Gaussian, the forces and response probability deviates from the Gaussian one. For the OWC case, this occurs because the force and response have quadratic transformations of the Gaussian process and non-symmetric viscous drag contribution. As a result, the exact response distribution of this problem is unknown.

Since part of the distribution is already Gaussian because of the wave elevation, it is reasonable to approximate the response by using a Gram–Charlier expansion of the Gaussian distribution (Johnson and Kotz, 1972). In this regard, the transfer function that describes the water column dynamics can be used to produce the PSD and calculate the central moments of the non-Gaussian response (Bedrosian and Rice, 1971). The response distribution can be calculated as (Donley and Spanos, 1990):

$$\mathrm{p}(\hat{\zeta}) = \left\{1 - \frac{1}{6}\mu_{\hat{\zeta}^3}\frac{\partial^3}{\partial\hat{\zeta}^3}\right\}\frac{1}{\sqrt{2\pi\mu_{\hat{\zeta}^2}}}\exp\left(-\frac{\hat{\zeta}}{2\mu_{\hat{\zeta}^2}}\right). \tag{27}$$

Due to the symmetry relations of the quadratic transfer functions (QTFs), the central moments can be obtained as:

$$\begin{aligned} \mu_{\hat{\zeta}^2} = &\int_{-\infty}^{\infty}\left|\mathrm{H}_{\hat{\zeta}}^{(1)}(\omega)\right|^2 S_{\xi\xi}(\omega)d\omega \\ &+ 2\iint_{-\infty}^{\infty}\left|\mathrm{H}_{\hat{\zeta}}^{(2)}(\omega_1,\omega_2)\right|^2 S_{\xi\xi}(\omega_1)S_{\xi\xi}(\omega_2)d\omega_1 d\omega_2, \end{aligned} \tag{28}$$

and:

$$\begin{aligned} \mu_{\hat{\zeta}^3} = &\,6\iint_{-\infty}^{\infty}\mathrm{H}_{\hat{\zeta}}^{(1)*}(\omega_1)\mathrm{H}_{\hat{\zeta}}^{(1)*}(\omega_2)\mathrm{H}_{\hat{\zeta}}^{(2)}(\omega_1,\omega_2) \\ &\times S_{\xi\xi}(\omega_1)S_{\xi\xi}(\omega_2)d\omega_1 d\omega_2 \\ &+ 8\iiint_{-\infty}^{\infty}\mathrm{H}_{\hat{\zeta}}^{(2)*}(\omega_1,\omega_2)\mathrm{H}_{\hat{\zeta}}^{(2)}(\omega_1,\omega_{-3})\mathrm{H}_{\hat{\zeta}}^{(2)}(\omega_2,\omega_3) \\ &\times S_{\xi\xi}(\omega_1)S_{\xi\xi}(\omega_2)S_{\xi\xi}(\omega_3)d\omega_1 d\omega_2 d\omega_3, \end{aligned} \tag{29}$$

where $S_{\xi\xi}(\omega)$ is the wave spectrum. The same procedure can be extended to calculate the probability distribution of the water column surface velocity, in order to calculate the equivalent linear and quadratic viscous drag term in Eq. (11). The probability distribution of the water column surface displacement, given in Eq. (27), is estimated using the second and third central moments, while the minimisation procedure, in Eq. (11), requires the fourth central moment. Based on that, the fourth central moments can be approximated to the ones of a Gaussian distribution by the following relationship (Donley and Spanos, 1990):

$$\mu_{\hat{\zeta}^4} = 3(\mu_{\hat{\zeta}^2}). \tag{30}$$

2.1.2. Iterative procedure

The determination of the first and second-order response depends on the prior knowledge of the probability distribution to estimate the equivalent linear and quadratic coefficients. Since this problem has no analytical solution, an iterative procedure can be used to estimate the water column response. In this regard, the step-by-step procedure described in Fig. 2 can be applied:

2.2. Statistical linearisation

For comparison purposes, this subsection briefly introduces the method of statistical linearisation (SL). In the SL approach, the nonlinear system is approximated to an equivalent linear one, where the difference between both equations is minimised in a mean square sense. Based on that, the governing equation is described based on Eq. (1), where only the linear forcing term is considered:

$$(\zeta+H)\ddot{\zeta} + C(\zeta+H)\dot{\zeta} + \frac{1}{2}C_V\dot{\zeta}\left|\dot{\zeta}\right| + g\zeta = g\xi - \left[\varphi_{w_l}\right]_{S_R}, \tag{31}$$

Like the SQ procedure, the mean surface displacement is estimated by taking the expectation of the main loads,

$$\mu_\zeta = g^{-1}\left\langle -\zeta\ddot{\zeta} - \frac{1}{2}C_V\dot{\zeta}\left|\dot{\zeta}\right|\right\rangle. \tag{32}$$

Here, it is important to highlight that $\langle\zeta\ddot{\zeta}\rangle = -\int\omega^2 S_{\zeta\zeta}d\omega$ is negative due to the phase between the displacement and acceleration, while $\langle\dot{\zeta}^2\rangle = \int\omega^2 S_{\zeta\zeta}d\omega$ is positive due to the quadratic transformation of

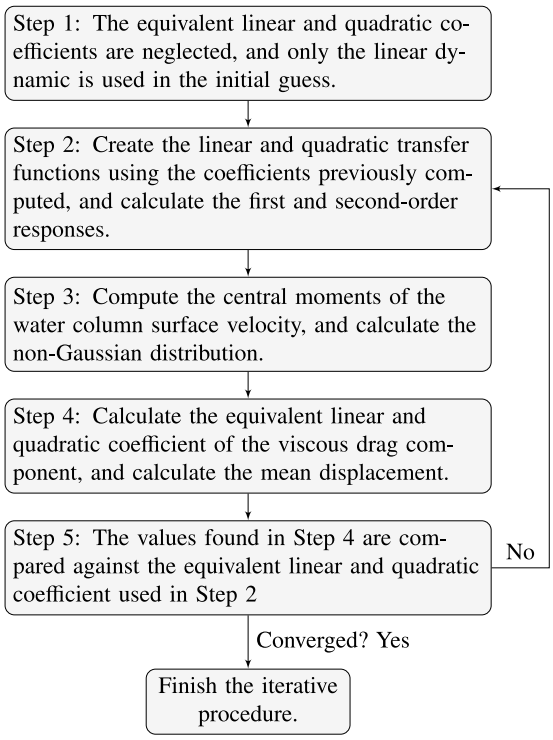

Fig. 2. Flowchart of the step-by-step procedure.

the velocity. Subtracting the mean displacement, the equivalent linear water column dynamics can be expressed as:

$$(H + H_{eq})\ddot{\xi} + H(C + C_{eq})\dot{\xi} + \frac{1}{2}C_V\dot{\xi}\left|\dot{\xi}\right| + (g + g_{eq})\xi = g\xi - \left[\varphi_{w_I}\right]_{S_R}, \quad (33)$$

where the subscript $_{eq}$ denotes the equivalent linear term obtained via SL by minimising the difference between the nonlinear equation and the equivalent one in a mean square sense. The equivalent terms can be obtained systematically, following the derivations in Roberts and Spanos (2003). For a Gaussian distribution, the minimisation condition to obtain the water column equivalent terms are given by:

$$H_{eq} = \left\langle \frac{\partial(\zeta\ddot{\zeta})}{\partial\ddot{\zeta}} \right\rangle = \mu_\zeta, \quad (34)$$

$$C_{eq} = \frac{C}{H}\left\langle \frac{\partial(\zeta\dot{\zeta})}{\partial\dot{\zeta}} \right\rangle + \frac{1}{2H}\left\langle C_V\frac{\partial(|\dot{\zeta}|\dot{\zeta})}{\partial\dot{\zeta}} \right\rangle = \frac{C}{H}\mu_\zeta + \frac{\overline{C_V}}{2H}\left(\frac{8}{\pi}\right)^{1/2}\sigma_{\dot{\zeta}}, \quad (35)$$

$$g_{eq} = \left\langle \frac{\partial(\zeta\ddot{\zeta})}{\partial\zeta} \right\rangle + C\left\langle \frac{\partial(\zeta\dot{\zeta})}{\partial\zeta} \right\rangle = 0, \quad (36)$$

where, $\overline{C_V}$ is the mean value of the heuristic damping coefficient, and $\sigma_{\dot{\zeta}}$ is the standard velocity of the water column surface. The equivalent transfer function that relates the water column displacement and the wave forces is given by:

$$\mathrm{H}(\omega) = \left[-\omega^2(H + \mu_\zeta) + i\omega H\left(C + C_{eq}\right) + g\right]^{-1}. \quad (37)$$

The SL procedure is conducted in a similar form as the SQ, however considering just first-order terms, having an analytical solution as shown in Eqs. (34) to (36). It is important to note that the quadratic water column nonlinearities are included in the SL model through the mean surface displacement. Obtaining an equivalent mass is usually recurrent when dealing with the nonlinear water column dynamics, as shown in Spanos et al. (2017, 2018) and Silva et al. (2019). As a result, the SL formulation shifts the apparent natural frequency of the water column when the equivalent linear system is perturbed by the incoming random wave field, which can be approximated to:

$$\omega_{n,eq} = \sqrt{\frac{g}{H + \mu_\zeta}}. \quad (38)$$

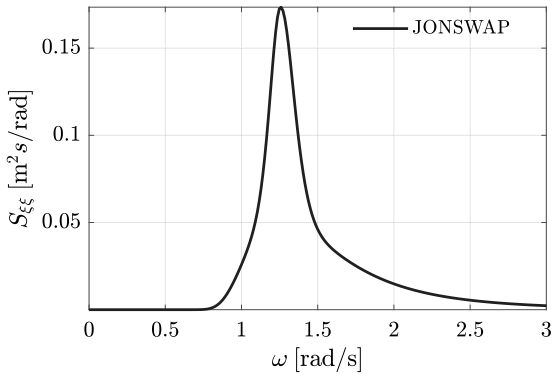

Fig. 3. Equivalent one-sided JONSWAP spectrum (T_p = 5 s, H_s = 1.5 m).

3. Simulations

Ocean waves have a random behaviour with energy content spread over a broad range of frequencies, which can be represented by means of spectral formulations. In this work, the incident wave field is assumed to be described by the JONSWAP formulation (Hasselmann et al., 1973), in which the equivalent one-sided spectrum form can be formulated as:

$$S_{\xi\xi}(\omega) = 320\frac{H_s^2}{T_p^4}\omega^{-5}\exp\left(-\frac{1950}{T_p^4}\omega^{-4}\right)\gamma^A, \quad (39)$$

with the enhancement peak factor $\gamma = 3.3$ and

$$A = \exp\left\{-\left(\frac{\omega/\omega_p - 1}{\sigma\sqrt{2}}\right)^2\right\}, \quad (40)$$

where, $\sigma = 0.07$ for $\omega < \omega_p$, and $\sigma = 0.09$ for $\omega > \omega_p$; H_s denotes the significant wave height; T_p is the wave peak period, which is related to the wave peak frequency by:

$$\omega_p = \frac{2\pi}{T_p}. \quad (41)$$

The wave spectrum is constructed from 200 frequency components varying from 0 to 2 rad/s for the TD and SL models, while 400 frequencies are used for the double-sided spectrum in the SQ formulation. It is worth noting that a suitable frequency discretisation is necessary to capture the effect of the sum and difference frequency components of the second-order response. Fig. 3 illustrates the equivalent one-sided JONSWAP spectrum.

For O&G and FOWTs applications, the water columns are designed to have their natural frequencies outside the sea spectrum range to avoid its resonance; while for wave energy applications, the natural frequency is designed close to the ones from the dominant wave peak period. To illustrate the response of OWCs under distinguished conditions, three water columns drafts are investigated, $H = [6, 12, 18]$ m; and two environmental conditions are simulated for each OWC configuration, one at $\omega_n \approx \omega_p$ (resonance) given in Table 2, and one at $\omega_n \approx 2\omega_p$ given in Table 4. Based on Eq. (38), the natural frequency of the water column for the undisturbed condition is given by:

$$\omega_n = \sqrt{\frac{g}{H}}. \quad (42)$$

The 2:1 ratio is analysed due to the quadratic effects of the loads, which generate sum and difference frequency components, while the resonance condition is analysed due to the wave energy applications. It is valuable to mention that the contribution of the nonlinear terms is higher for water columns with short draft and the magnitude of the wave forcing terms are higher. The main parameters of the simulation are given in Table 1. Note that the heuristic damping coefficients

Table 1
Simulation parameters.

Property	Value	Unit
ρ	1025	[kg/m^3]
C_V ($\dot{\hat{\zeta}} > 0$)	0.3	[–]
C_V ($\dot{\hat{\zeta}} < 0$)	0.5	[–]
C	0.05	[s^{-1}]
h	200	[m]
g	9.81	[m/s^2]

Table 2
OWC parameters and sea conditions ($\omega_n \approx \omega_p$).

Property	Case 1	Case 2	Case 3	Unit
H	6	12	18	[m]
ω_n	1.27	0.9	0.74	[rad/s]
H_s	1.5	3	4.5	[m]
T_p	5	7	8.5	[s]
ω_p	1.25	0.9	0.74	[rad/s]

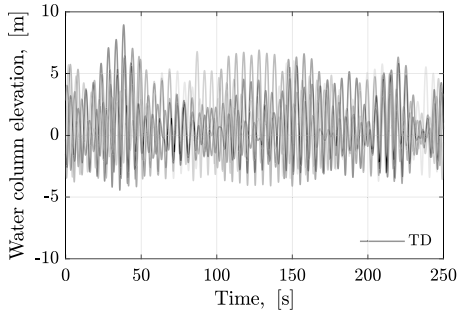

Fig. 4. Time series of five water column elevations using nonlinear TD simulations for the first 250 s of the stead-state data using different phase angles in the wave spectrum (T_p = 5 s, H_s = 1.5 m and H = 6 m).

need to be calibrated using experimental data and computational fluid dynamics.

The reliability of both statistical methods is assessed by comparing their results with those obtained from nonlinear TD simulations. The simulations are obtained over an interval of 5000 s at a sampling frequency of 40 Hz. Also, each environmental condition is performed 30 times using different sets of wave random phase angles due to the sensitivity of the second-order response of TD simulations. Fig. 4 illustrates a time series of five water column elevations using different phase angles for wave spectrum (T_p = 5 s, H_s = 1.5 m). As can be observed, there is an asymmetry in the water column elevation due to the presence of nonlinearities, which is more pronounced depending on the random phase used to create the sea surface elevation.

Consider the water column drafts and sea states given in Table 2, where the natural frequency of the OWCs coincides with the incoming wave field ($\omega_n \approx \omega_p$). This condition is referred to as resonance, leading to an increase in water column oscillations, and is characterised by a peak in the spectral response. Figs. 5 to 7(a) show the water column spectral response obtained via SQ, SL and TD models. The TD results in Figs. 5 to 7(a) are obtained using the *pwelch* function in MATLAB, where the results in grey refer to the 30 nonlinear TD simulations using different sets of random wave components, and the result in blue refer to their mean value. For the SQ approach, the PSD of the water column displacement is calculated as follows:

$$S_{\hat{\zeta}\hat{\zeta}}(\omega) = \left|\mathrm{H}^{(1)}_{\hat{\zeta}}(\omega)\right|^2 S_{\xi\xi}(\omega) + 2\int_{-\infty}^{\infty}\left|\mathrm{H}^{(2)}_{\hat{\zeta}}(\omega_1, \omega-\omega_1)\right|^2 S_{\xi\xi}(\omega_1) S_{\xi\xi}(\omega-\omega_1) d\omega_1, \tag{43}$$

while for SL, only the first term on the right-hand side of Eq. (43) is computed, with its respective transfer function given in Eq. (37). Since the OWCs are operating in resonance, the first-order response is characterised by a single peak around the natural frequency which is captured by all models (TD, SL, and SQ). As expected, the SL model is limited to the response spectrum at large energy densities, which occurs at the sea spectrum range. On the other hand, the SQ method recovered the energy spectrum of the water column elevation obtained with TD simulations over the first and second-order effects. The peaks at higher frequencies on the right of the first-order response are associated with second-order effects related to frequency-sums combinations (2:1 resonance), while low-frequency responses on the left of first-order responses are related to the frequency-differences combinations that generate slow displacements of the water column elevation. Higher-order responses are observed in the TD responses that are only captured using higher-order models. However, it is important to note that the contribution of higher-order responses is reduced.

Figs. 5 to 7(b) show the histogram of the water column displacement using TD and the PDFs estimated using SQ and SL techniques. Due to the high energy at first-order responses, all methods have a similar standard deviation. The main differences occur at the tail of the distribution and asymmetry (skewness), which are captured using SQ and TD models. The skewness in the PDF is due to the presence of second-order responses, where the main sources of loads are described in Figs. 5 to 7(c). As it can be observed, the nonlinearity related to the variable mass plays an important role in the second-order motion, being a few orders of magnitude higher than other second-order non-linearities and comparable to the first-order wave excitation. Note that there is a physical singularity in this simple model, establishing the domain of validity when the water column approximates the lower limit ($\zeta \rightarrow -H$). For such conditions, the mass tends to zero, the variable fluid mass becomes null, and the system responds faster to the restoring force, raising the asymmetry in the PDF of the water column displacement, which was demonstrated in Fig. 4. Since Eqs. (15) and (16) have the same linear differential operator, the PSD of the water column displacement can be calculated from the PSD of the forces as:

$$S_{\hat{\zeta}\hat{\zeta}}(\omega) = |\mathrm{H}(\omega)|^2 S_{\hat{f}\hat{f}}(\omega), \tag{44}$$

where:

$$S_{\hat{f}\hat{f}}(\omega) = \left|\mathrm{H}^{(1)}_{\hat{f}}(\omega)\right|^2 S_{\xi\xi}(\omega) + 2\int_{-\infty}^{\infty}\left|\mathrm{H}^{(2)}_{\hat{f}}(\omega_1, \omega-\omega_1)\right|^2 S_{\xi\xi}(\omega_1) S_{\xi\xi}(\omega-\omega_1) d\omega_1, \tag{45}$$

which are shown in Figs. 5 to 7(c). As in the response spectrum, only the first term on the right-hand side of Eq. (45) is computed in the force spectrum for the SL technique.

Since the high energy of the response spectrum (oscillating water column displacement) occurs at first-order responses (wave frequency range), all methods and simulations have a similar standard deviation. The main differences occur at the tail of the distribution and asymmetry (skewness), which are only captured using SQ and TD models. The central moments used to calculate the PDF in Figs. 5 to 7(b) are reported in Table 3. The skewness in the PDF is due to the presence of second-order responses, where the main sources of loads are described in Figs. 5 to 7(c).

In the second analysis, consider the water column drafts and sea states given in Table 4, where the natural frequency of the OWCs is approximately two times the wave peak frequency ($\omega_n \approx 2\omega_p$). Figs. 8 to 10(a) show the water column spectral response obtained via SQ, SL and TD models, where the first-order response is characterised by a bimodal spectrum. The first peak in the spectral responses occurs due to the incoming wave field, while the second peak is associated with the natural frequency of the OWCs. As stated previously, the SL is limited to the primary range of excitation and the response spam over the wave frequency, while the SQ accounts for second-order responses. Higher-order responses can be observed in the TD model; however, their contributions are small for the conditions simulated.

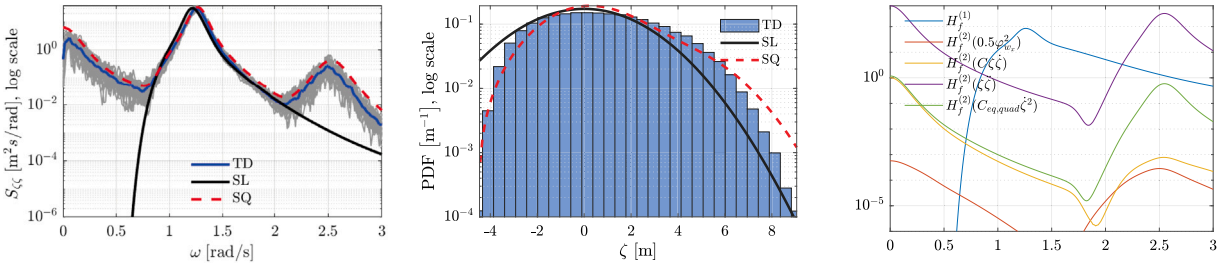

(a) PSD of the water column elevation (b) PDF of the water column elevation (c) PSD of the forcing terms (SQ)

Fig. 5. Water column dynamics when $\omega_n \approx \omega_p$ (T_p = 5 s, H_s = 1.5 m, and H = 6 m).

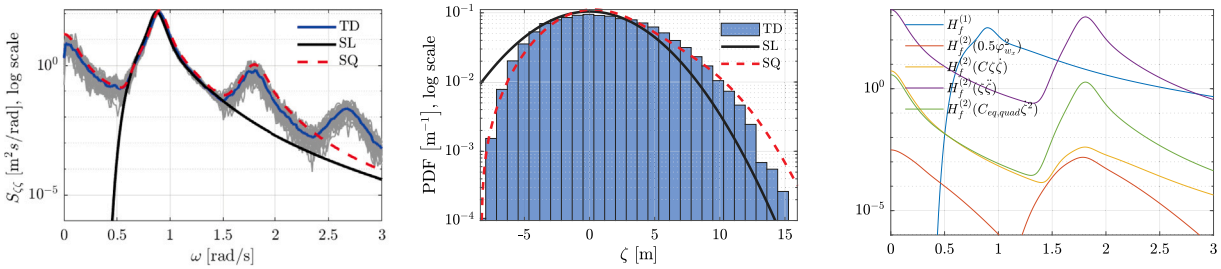

(a) PSD of the water column elevation (b) PDF of the water column elevation (c) PSD of the forcing terms (SQ)

Fig. 6. Water column dynamics when $\omega_n \approx \omega_p$ (T_p = 7 s, H_s = 3 m and H = 12 m).

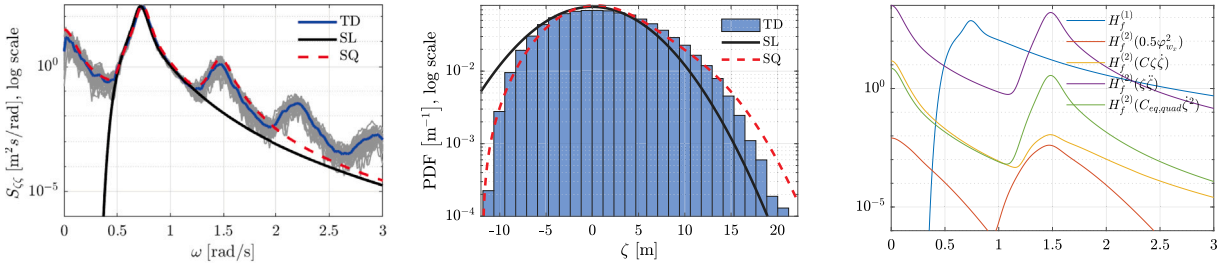

(a) PSD of the water column elevation (b) PDF of the water column elevation (c) PSD of the forcing terms (SQ)

Fig. 7. Water column dynamics when $\omega_n \approx \omega_p$ (T_p = 8.5 s, H_s = 4.5 m and H = 18 m).

Table 3
Central moments using TD, SL and SQ methods across all environmental conditions in Table 2.

H [m]	Variable	TD	SL	SQ	Unit
6	μ_{ξ_1}	0.83 ± 0.02	0.86	0.93	[m]
	μ_{ξ_2}	5.57 ± 0.13	5.35	4.84	[m^2]
	μ_{ξ_3}	3.91 ± 0.56	0	8.18	[m^3]
12	μ_{ξ_1}	1.17 ± 0.04	1.22	1.33	[m]
	μ_{ξ_2}	15.32 ± 0.44	14.62	14.04	[m^2]
	μ_{ξ_3}	19.17 ± 4.28	0	33.51	[m^3]
18	μ_{ξ_1}	1.46 ± 0.05	1.53	1.66	[m]
	μ_{ξ_2}	28.32 ± 0.83	26.98	26.44	[m^2]
	μ_{ξ_3}	47.02 ± 13.29	0	79.21	[m^3]

Figs. 8 to 10(b) show the histogram of the water column displacement using TD and the PDFs estimated using SQ and SL techniques, where the SQ model has a better agreement with TD simulations.

The main idea of these conditions ($\omega_n \approx 2\omega_p$) is to analyse the effect of second-order forces, more specifically, the sum-frequency components, on the overall response. However, since the main source of nonlinearity comes from the inertial term and the water columns were not resonating, the nonlinear effects and second-order responses were lower compared to the case given in Table 2, which are shown in Figs. 8 to 10(c). The second-order response depends on the results of the bimodal first-order response and their interactions, which produced a smoother spectral response curve. Like the previous cases, the variable mass is the main source of nonlinearity related to second-order motion. It is important to highlight that the second-order loads were lower than for the previous environmental conditions. This happened because the responses occurred at lower frequencies and most nonlinear terms are described as a function of the acceleration and velocity, which are smaller at lower frequencies. Moreover, the nonlinearities are more pronounced for shorter water columns at resonance, since their response occurs at higher frequencies.

Table 4
OWC parameters and sea conditions ($\omega_n \approx 2\omega_p$).

Property	Case 1	Case 2	Case 3	Unit
H	6	12	18	[m]
ω_n	1.27	0.9	0.74	[rad/s]
H_s	1.5	3	4.5	[m]
T_p	10	13.5	17	[s]
ω_p	0.63	0.46	0.37	[rad/s]

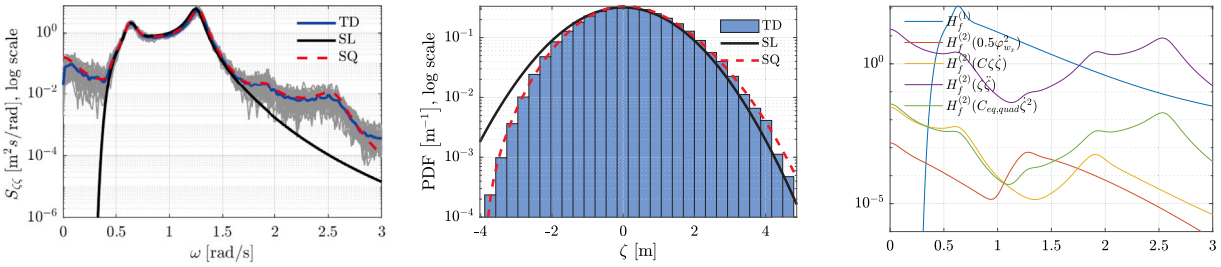

(a) PSD of the water column elevation (b) PDF of the water column elevation (c) PSD of the forcing terms (SQ)

Fig. 8. Water column dynamics when $\omega_n \approx 2\omega_p$ (T_p = 10 s, H_s = 1.5 m and H = 6 m).

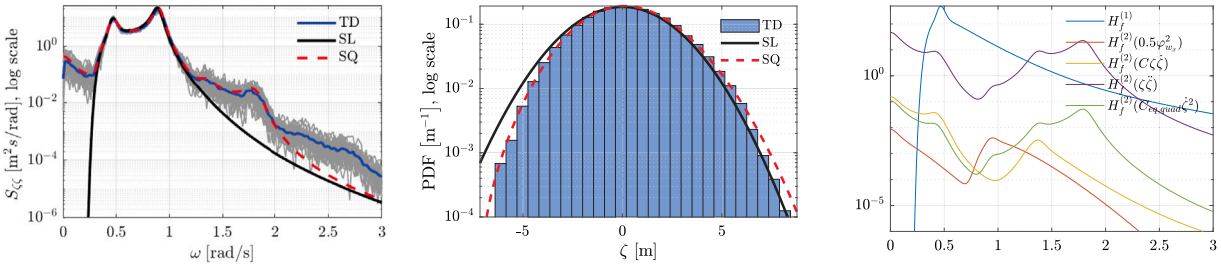

(a) PSD of the water column elevation (b) PDF of the water column elevation (c) PSD of the forcing terms (SQ)

Fig. 9. Water column dynamics when $\omega_n \approx 2\omega_p$ (T_p = 13.5 s, H_s = 3 m and H = 12 m).

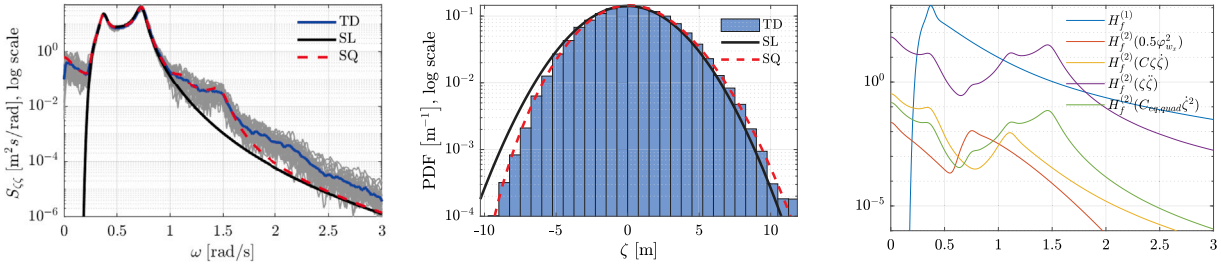

(a) PSD of the water column elevation (b) PDF of the water column elevation (c) PSD of the forcing terms (SQ)

Fig. 10. Water column dynamics when $\omega_n \approx 2\omega_p$ (T_p = 17 s, H_s = 4.5 m and H = 18 m).

Table 5
Central moments using TD, SL and SQ methods across all environmental conditions in Table 4.

H [m]	Variable	TD	SL	SQ	Unit
6	$\mu_{\hat{\zeta}^1}$	0.17 ± 0.01	0.20	0.19	[m]
	$\mu_{\hat{\zeta}^2}$	1.46 ± 0.06	1.57	1.45	[m^2]
	$\mu_{\hat{\zeta}^3}$	0.32 ± 0.12	0	0.36	[m^3]
12	$\mu_{\hat{\zeta}^1}$	0.26 ± 0.01	0.29	0.28	[m]
	$\mu_{\hat{\zeta}^2}$	4.32 ± 0.12	4.58	4.33	[m^2]
	$\mu_{\hat{\zeta}^3}$	1.27 ± 0.64	0	1.50	[m^3]
18	$\mu_{\hat{\zeta}^1}$	0.29 ± 0.01	0.32	0.31	[m]
	$\mu_{\hat{\zeta}^2}$	7.70 ± 0.24	7.95	7.62	[m^2]
	$\mu_{\hat{\zeta}^3}$	2.86 ± 1.84	0	2.79	[m^3]

The central moments used to calculate the PDF in Figs. 8 to 10(b) are reported in Table 5. Like the previous condition ($\omega_n \approx \omega_p$), SL and SQ methods obtained good accuracy in calculating the first two central moments of the water column surface elevation, while only the SQ model is capable of calculating third central moments. The accuracy of the SQ for the second environmental condition given in Table 4 was superior to the first case, because the strength of the nonlinearities arises under resonance, reducing the accuracy of the method.

3.1. Computational cost

The SQ provides reliable estimations of the first and second-order response of the water column dynamics which are comparable to nonlinear TD simulations, as observed in the PSD and PDF results. However, since it is a frequency domain approach, the required computational demand is the main advantage of the SQ method over TD simulations. Table 6 shows the mean simulation clock time over all simulations performed for the different approaches used in this work, namely the SQ, SL, and TD models. The simulations were performed using a standard desktop PC with an Intel Core i7 processor (2.4 GHz) and 16 GB RAM. The main characteristics of the TD, SL, and SQ models are described in Section 3.

In general, 3–5 iterations were required for the SQ and SL models to obtain a relative error of 0.1% between the central moments of the previous iteration step. Each TD simulation required approximately 82.1 s; however, several sets of angles were used to construct the wave elevation in order to reduce the sensitivity of the random phase angle in the second-order response. Hence, the SQ is approximately two orders of magnitude faster than TD simulations, which agrees with the results given in Donley and Spanos (1990). However, it is important to note that the frequency discretisation directly affects the simulation

Table 6
Comparison of mean simulation clock time.

Model	Clock time	Unit
SL	0.01	[s]
SQ	2.92	[s]
TD	82.1	[s]

clock time of the SQ method, especially when calculating the third-order moments (triple integrals). Also, the computational time required using TD simulations is dependent on the number of frequencies and simulation time and discretisation.

This article aims to model and demonstrate the accuracy of the SQ applied to OWCs. Therefore, a better comparison between the models is necessary to investigate the efficiency and accuracy balance between models. In this regard, a discretisation study of the spectrum is important in order to have reasonable computational clock time and reliable estimation of second-order effects. During design optimisation processes, since the SL provided good estimates of the first two central moments, it can still be used as a first assessment of the OWC design and better models at further stages.

4. Conclusion

This work investigated the nonlinear stochastic dynamics of OWCs using statistical linearisation. Firstly, the paper introduced the main sources of nonlinearities and demonstrated the derivation of an SQ model. Then, the capability of the SQ model was demonstrated against the SL model and nonlinear TD simulations. The OWCs were subjected to two environmental conditions, namely, when $\omega_n \approx \omega_p$, and $\omega_n \approx 2\omega_p$, and their dynamics were discussed regarding differences observed between numerical models.

In general, the SL model provided reasonable estimates of the mean and mean-square responses of WECs. However, the model is restricted to first-order dynamics and Gaussian distributions. As a result, equivalent linear responses from SL might lose salient features of the actual nonlinear dynamics. It is well known that nonlinearities may lead to vibrations outside the excitation range frequency, and the real response may lead to a non-Gaussian distribution. These limitations can be addressed using SQ, where the nonlinearities are described by linear and quadratic transfer functions. The main advantage of including these second-order terms is the possibility of estimating the effects of non-symmetric loads (described by even functions). The quadratic transfer functions generate low-frequency and high-frequency loads (second-order loads) given by the difference and the sum of the frequency components, respectively. Also, quadratic transfer functions can be used to calculate higher central moments to create Non-Gaussian distributions using Gram–Charlier expansions of the Gaussian distribution. Therefore, the SQ model was capable of providing better estimates of the PSD and PDF responses of the water column surface displacement than the SL model.

It is important to remind the reader that the equivalent terms obtained from SQ differ from the ones obtained with SL, and are calculated for each design and environmental condition. The significance of the quadratic transfer functions is dependent on the frequency distribution and the degree of non-symmetry of the nonlinearity. Therefore, in the case of symmetric nonlinearities, the quadratic terms are null and the SQ reduces to the SL. In this work, only the water column surface elevation was modelled. However, it can be extended to more degrees of freedom and other sources of nonlinearities by making the appropriate modifications (Donley and Spanos, 1990).

For the OWC investigated in this work, the nonlinearity from the variable mass system was the main source of load related to second-order motion. It is important to highlight that the second-order effects were lower when $\omega_n \approx 2\omega_p$ than when $\omega_n \approx \omega_p$. This happened because the responses are higher when the OWCs operate in resonance ($\omega_n \approx \omega_p$), having higher nonlinearities. In addition, since some nonlinear terms are described as a function of acceleration and velocity, the response at low frequencies results in smaller nonlinear loads. Note that the nonlinearities were more pronounced for shorter water columns at resonance, since their response occurs at higher frequencies. It is important to highlight that when OWCs are applied to wave energy harvesting, the power take-off system and the chamber dynamics offer additional damping to the system, which may reduce the intensity of the nonlinear effects when compared with the simulations presented, leading to better agreements between SQ and TD models.

CRediT authorship contribution statement

L.S.P. da Silva: Conceptualization, Methodology, Software, Investigation, Validation, Formal analysis, Writing – original draft, Visualization. **C.P. Pesce:** Conceptualization, Methodology, Investigation, Formal analysis, Writing – review & editing, Supervision. **M. de Oliveira:** Investigation, Writing – review & editing. **N.Y. Sergiienko:** Writing – review & editing, Supervision. **B. Cazzolato:** Writing – review & editing, Supervision. **B. Ding:** Writing – review & editing, Supervision.

Declaration of competing interest

The authors declare that they have no known competing financial interests or personal relationships that could have appeared to influence the work reported in this paper.

Data availability

No data was used for the research described in the article.

Acknowledgements

L. S. P. da Silva acknowledges Delmar Systems, the Australia-China Science and Research Fund, Australian Department of Industry, Innovation and Science; and the Adelaide Graduate Centre, the University of Adelaide. C. P. Pesce acknowledges CNPq - Brazilian National Research Council grant, process n. 307995/2022-4. M. de Oliveira acknowledges FUSP, the Foundation of Support to the University of São Paulo - Process number 392802. The FAPESP, São Paulo Research Foundation, thematic project 'Nonlinear Dynamics Applied to Engineering', process nr 2022/00770-0 is also acknowledged.

References

Aalbers, A., 1984. The water motions in a moonpool. Ocean Eng. 11 (6), 557–579.
Bedrosian, E., Rice, S.O., 1971. The output properties of Volterra systems (nonlinear systems with memory) driven by harmonic and Gaussian inputs. Proc. IEEE 59 (12), 1688–1707.
Casetta, L., Pesce, C.P., 2013. The generalized Hamilton's principle for a non-material volume. Acta Mech. 224 (4), 919–924.
Chuang, T.-C., Yang, W.-H., Yang, R.-Y., 2021. Experimental and numerical study of a barge-type FOWT platform under wind and wave load. Ocean Eng. 230, 109015.
da Silva, L.S.P., 2019. Nonlinear stochastic analysis of wave energy converters via statistical linearization Master's thesis. University of São Paulo, Brazil.
da Silva, L.S.P., 2023. Stochastic Analysis of Marine Renewable Energy Devices: Wave, Wind, and Hybrid Systems (Ph.D. thesis). University of Adelaide, Adelaide, Australia.
da Silva, L.S., Ding, B., Guo, B., Sergiienko, N.Y., 2022a. Wave energy converter modelling, control, and power take-off design. In: Modelling and Optimisation of Wave Energy Converters. CRC Press, pp. 97–128.
da Silva, L.S.P., de Oliveira, M., Cazzolato, B., Sergiienko, N., Amaral, G.A., Ding, B., 2022b. Statistical linearisation of a nonlinear floating offshore wind turbine under random waves and winds. Ocean Eng..
da Silva, L.S.P., Sergiienko, N.Y., Cazzolato, B., Ding, B., 2022c. Dynamics of hybrid offshore renewable energy platforms: Heaving point absorbers connected to a semi-submersible floating offshore wind turbine. Renew. Energy 199.
Davidson, J., Costello, R., 2020. Efficient nonlinear hydrodynamic models for wave energy converter design—A scoping study. J. Mar. Sci. Eng. 8 (1), 35.
Donley, M.G., Spanos, P., 1990. Dynamic Analysis of Non-Linear Structures By the Method of Statistical Quadratization. vol. 57, Springer Science & Business Media.

Falcão, A.F., Henriques, J.C., 2016. Oscillating-water-column wave energy converters and air turbines: A review. Renew. Energy 85, 1391–1424.
Folley, M., 2016. Spectral-domain models. In: Folley, M. (Ed.), Numerical Modelling of Wave Energy Converters: State-of-the-Art Techniques for Single Devices and Arrays. Academic Press, pp. 67–80.
Folley, M., Whittaker, T., 2013. Validating a spectral-domain model of an OWC using physical model data. Int. J. Mar. Energy 2, 1–11.
Guo, X., Lu, H., Yang, J., Peng, T., 2017. Resonant water motions within a recessing type moonpool in a drilling vessel. Ocean Eng. 129, 228–239.
Hasselmann, K.F., Barnett, T.P., Bouws, E., Carlson, H., Cartwright, D.E., Eake, K., Euring, J., Gicnapp, A., Hasselmann, D., Kruseman, P., Meerburg, A., Muller, P., Olbers, D.J., Richter, K., Sell, W., Walden, H., 1973. Measurements of wind-wave growth and swell decay during the Joint North Sea Wave Project (JONSWAP).. Ergaenzungsheft Dtsch. Hydrogr. Z. Reihe A.
Ideol, B., 2022. Floating offshore wind - BW Ideol. URL http://www.bw-ideol.com.
Johnson, N.L., Kotz, S., 1972. Distributions in Statistics: Continuous Multivariate Distributions. John Wiley & Sons, New York, pp. 10–12.
Karimi, M., Buckham, B., Crawford, C., 2019. A fully coupled frequency domain model for floating offshore wind turbines. J. Ocean Eng. Mar. Energy 5 (2), 135–158.
Li, A.-J., Liu, Y., 2019. New analytical solutions to water wave diffraction by vertical truncated cylinders. Int. J. Naval Archit. Ocean Eng. 11 (2), 952–969.
Li, X.-M., Quek, S.-T., Koh, C.-G., 1995. Stochastic response of offshore platforms by statistical cubicization. J. Eng. Mech. 121 (10), 1056–1068.
Li, L., Ruzzo, C., Collu, M., Gao, Y., Failla, G., Arena, F., 2020. Analysis of the coupled dynamic response of an offshore floating multi-purpose platform for the blue economy. Ocean Eng. 217, 107943.
Malara, G., Spanos, P.D., 2019. Efficient determination of nonlinear response of an array of oscillating water column energy harvesters exposed to random sea waves. Nonlinear Dynam. 98, 2019–2034.
Masetti, I.Q., Costa, A.P.d.S., Sphaier, S.H., Nishimoto, K., Machado, G., 2012. Development of a concept of mono–column platform: MONOBR. Int. J. Comput. Appl. Technol. 43 (3), 225–233.
Pesce, C., 2003. The application of Lagrange equations to mechanical systems with mass explicitly dependent on position. J. Appl. Mech. 70 (5), 751–756.
Pesce, C.P., Orsino, R.M.M., da Silva, L.S.P., 2023. Nonlinear dynamics of variable mass oscillators. In: Lectures on Nonlinear Dynamics, Chapter 8. Eds. Piqueira, J.R., Mazzilli, C.E.N., Pesce, C.P., Franzini, G.R.. Springer Nature.
Quek, S., Li, X., Koh, C., 1994. Stochastic response of jack-up platform by the method of statistical quadratization. Appl. Ocean Res. 16 (2), 113–122.
Roberts, J.B., Spanos, P.D., 2003. Random Vibration and Statistical Linearization. Courier Corporation.
Sanchez-Mondragon, J., Vázquez-Hernández, A., Cho, S., Sung, H., 2017. Motion behavior in a turret-moored FPSO caused by piston mode effects in moonpool. Ocean Eng. 140, 222–232.
Scialò, A., Malara, G., Kougioumtzoglou, I.A., Arena, F., 2022. Stochastic response determination of U-OWC energy harvesters: a statistical linearization solution treatment accounting for intermittent wave excitation. Nonlinear Dynam. 1–15.
Silva, L.S.P., Cazzolato, B., Sergiienko, N., Ding, B., 2021. Nonlinear dynamics of a floating offshore wind turbine platform via statistical quadratization - mooring, wave and current interaction. Ocean Eng. 236, 1–13.
Silva, L.S.P., Pesce, C.P., Morishita, H.M., Gonçalves, R.T., 2019. Nonlinear analysis of an oscillating water column wave energy device in frequency domain via statistical linearization. In: ASME 2019 38th International Conference on Ocean, Offshore and Arctic Engineering. American Society of Mechanical Engineers, pp. 1–9.
Silva, L.S.P., Sergiienko, N., Pesce, C.P., Ding, B., Cazzolato, B., Morishita, H.M., 2020. Stochastic analysis of nonlinear wave energy converters via statistical linearization. Appl. Ocean Res. 95.
Socha, L., 2005a. Linearization in analysis of nonlinear stochastic systems: recent results—part I: theory. Appl. Mech. Rev. 58 (3), 178–205.
Socha, L., 2005b. Linearization in analysis of nonlinear stochastic systems, recent results—part II: applications. Appl. Mech. Rev. 58 (5), 303–315.
Socha, L., 2008. Linearization Methods for Stochastic Dynamic Systems. Springer, Berlin.
Spanos, P.D., 1981. Stochastic linearization in structural dynamics. Appl. Mech. Rev. 34 (1), 1–8.
Spanos, P., Donley, M., 1991. Equivalent statistical quadratization for nonlinear systems. J. Eng. Mech. 117 (6), 1289–1310.
Spanos, P.D., Ghosh, R., Finn, L.D., Halkyard, J., 2005. Coupled analysis of a spar structure: Monte Carlo and statistical linearization solutions. J. Offshore Mech. Arct. Eng. 127 (1), 11–16.
Spanos, P.D., Nava, V., Arena, F., 2011. Coupled surge-heave-pitch dynamic modeling of spar-moonpool-riser interaction. J. Offshore Mech. Arctic Eng. 133 (2).
Spanos, P.D., Strati, F.M., Malara, G., Arena, F., 2017. Stochastic dynamic analysis of U-OWC wave energy converters. In: ASME 2017 36th International Conference on Ocean, Offshore and Arctic Engineering. American Society of Mechanical Engineers, pp. 1–8.
Spanos, P.D., Strati, F.M., Malara, G., Arena, F., 2018. An approach for non-linear stochastic analysis of U-shaped OWC wave energy converters. Probab. Eng. Mech. 54, 44–52.
Taylor, R.E., Huang, J., 1997. Semi-analytical formulation for second-order diffraction by a vertical cylinder in bichromatic waves. J. Fluids Struct. 11 (5), 465–484.
Tognarelli, M.A., Zhao, J., Kareem, A., 1997a. Equivalent statistical cubicization for system and forcing nonlinearities. J. Eng. Mech. 123 (8), 890–893.
Tognarelli, M.A., Zhao, J., Rao, K.B., Kareem, A., 1997b. Equivalent statistical quadratization and cubicization for nonlinear systems. J. Eng. Mech. 123 (5), 512–523.